Published in final edited form as:
J Neuropathol Exp Neurol. 2010 September ; 69(9): 945–958. doi:10.1097/NEN.0b013e3181efa658.

Axonal Pathology Precedes Demyelination in a Mouse Model of X-Linked Demyelinating/ Type I Charcot-Marie Tooth (CMT1X) Neuropathy

Natalie Vavlitou, MSc, **Irene Sargiannidou, PhD**, **Kyriaki Markoullis, PhD**, **Kyriacos Kyriacou, PhD**, **Steven S. Scherer, MD, PhD**, and **Kleopas A. Kleopa, MD**
Neuroscience Laboratory and Neurology Clinics (NV, IS, KM, KAK) and Department of Electron Microscopy and Molecular Pathology (KK), The Cyprus Institute of Neurology and Genetics, Nicosia, Cyprus; and Department of Neurology, University of Pennsylvania School of Medicine (SSS), Philadelphia, Pennsylvania, PA

Abstract

X-linked Charcot-Marie-Tooth disease (CMT1X) is an inherited peripheral neuropathy caused by mutations in *GJB1*, the gene that encodes the gap junction protein connexin32 (Cx32). Cx32 is expressed by myelinating Schwann cells and forms gap junctions in non-compact myelin areas but axonal involvement is more prominent in X-linked compared to other forms of demyelinating Charcot-Marie-Tooth disease. To clarify the cellular and molecular mechanisms of axonal pathology in CMT1X, we studied *Gjb1*-null mice at early stages (i.e. 2- to 4-month-old) of the neuropathy, when there is minimal or no demyelination. The diameters of large myelinated axons were progressively reduced in *Gjb1*-null mice compared to those in wild type littermates. Furthermore, neurofilaments were relatively more dephosphorylated and more densely packed starting at 2 months of age. Increased expression of β-amyloid precursor protein, a marker of axonal damage, was also detected in *Gjb1*-null nerves. Finally, fast axonal transport, assayed by sciatic nerve ligation experiments, was slower in distal axons of *Gjb1*-null vs. wild type animals with reduced accumulation of synaptic vesicle-associated proteins. These findings demonstrate that axonal abnormalities including impaired cytoskeletal organization and defects in axonal transport precede demyelination in this mouse model of CMT1-X.

Keywords

Axonal degeneration; Axonal transport; Charcot-Marie Tooth; Connexin32; Cx32; Gap junctions; Neurofilaments

INTRODUCTION

Since the first report of Bergoffen et al (1), over 300 different *GJB1* mutations have been found to cause the X-linked demyelinating/type 1 form of Charcot-Marie-Tooth disease (CMT1X) (http://www.molgen.ua.ac.be/CMTMutations/default.cfm). *GJB1* encodes the gap junction (GJ) protein connexin32 (Cx32), which is thought to form GJs between the layers of non-compact myelin in peripheral nervous system (PNS) myelin sheaths (2–4). Patients with CMT1X develop a progressive length-dependent axonal loss that results in the clinical

Send correspondence and reprint requests to: Kleopas A. Kleopa, MD. The Cyprus Institute of Neurology and Genetics, P.O. Box 23462, 1683 Nicosia, Cyprus. Phone: +357-22-358600; Fax: +357-22-392786; kleopa@cing.ac.cy.
Natalie Vavlitou and Irene Sargiannidou contributed equally to this work.

picture of progressive muscle atrophy, weakness, and sensory loss in distal extremities (5). The electrophysiological and pathological findings in CMT1X patients suggest that there is less demyelination and more axonal loss compared to patients with other types of CMT1 (6–10). In CMT1X, as in other forms of CMT1, axonal degeneration and not demyelination appears to be the main cause of neurological disability (11).

Several animal models of CMT1 have provided insight into how demyelinating neuropathies evolve. In *Gjb1*-null mice, demyelination begins at around post-natal day 90 (P90), with subsequent axonal loss (12,13). In *Pmp22*-null (14), *Trembler* (15) and *TremblerJ* (16), as well as *Mpz*-null mice (17–18), demyelination has an even earlier onset, and distally accentuated axonal loss worsens over time. In demyelinated axons of *Trembler* mice, neurofilaments (NFs) are more densely packed and less phosphorylated and axonal transport is slower (19). Some of these abnormalities have also been found in nerves from patients with CMT1 (20). Transplantation of a segment of *Trembler* (21,22) or CMT1A (23) nerve into normalnerve also produces similar changes in axons that have regenerated through the nerve graft but not in the surrounding nerve, demonstratingthat this effect results from interactions with genetically abnormal Schwanncells. Finally, mutant Schwann cells from CMT1X patients transplanted into sciatic nerves of nude mice induced increased density of axonal neurofilaments, depletion of microtubules, and increased density of vesicles and mitochondria without demyelination (24).

How Cx32 mutations lead to early axonal dysfunction and degeneration in the absence of demyelination remains poorly understood. The aim of this study was to examine the onset and mechanisms of early axonal pathology in *Gjb1*-null mice. We chose this model of CMT1X neuropathy because our recent studies demonstrated that loss of function is the main mechanism of *GJB1* mutations (25). Furthermore, several clinical reports have shown similar disease severity in CMT1X patients with point mutations compared to complete deletion of the *GJB1* gene (26–28). We show here that before demyelination occurs, *Gjb1*-null mice have altered NFs, disturbed axonal transport, and increased expression of amyloid precursor protein (APP), a marker of axonal injury (29). These results provide evidence that the loss of Cx32 function in PNS myelin sheaths affects axons independently of demyelination.

MATERIALS AND METHODS

Transgenic Mice

Gjb1-null mice (C57BL/6x129) were obtained from the European Mouse Mutant Archive, Monterotondo, Italy (originally generated by Prof. Klaus Willecke, University of Bonn, Germany) (30). In these mice, the *neo*^{r} gene was inserted in frame into the exon 2 of *Gjb1* gene, which contains the open reading frame. Genotyping was performed using PCR screening with primers specific for the wild type (WT) *Gjb1* mouse gene as well as for the *neo*^{r} gene (*Gjb1*-null), as previously described (25). *Gjb1*-null mice were compared to their WT littermates at the ages of 2 and 4 months. Studies were also performed in 8-month-old mice to assess progression of axonal pathology.

Immunoblot Analysis

Sciatic nerves were dissected into the proximal (lumbar spine to the sciatic notch) and distal (sciatic notch to the knee) segments and lysed in ice-cold radioimmunoprecipitation assay (RIPA) buffer (10 mM sodium phosphate pH 7.0, 150 mM NaCl, 2 mM EDTA, 50 mM sodium fluoride, 1% NP-40, 1% sodium deoxycholate, and 0.1% SDS), containing a cocktail of protease inhibitors (Roche, Basel, Switzerland). For immunoblot analysis of NFs, samples were additionally treated with a cocktail of phosphatase inhibitors (Roche) to ensure

preservation of phosphorylation status. No difference in the yield of either SMI31 or SMI32 was observed when the same samples were processed with Laemmli (62.5 mM Tris pH6.8, 2% SDS) as opposed to RIPA buffer, and no significant amounts of NFs were retained in the RIPA-insoluble fraction (Supplemental Fig. 1). Protein lysates (30 μg) were fractionated by 8% SDS-polyacrylamide gel electrophoresis (SDS-PAGE) and transferred to a Hybond-C extra membrane (Amersham, Piscataway, NJ) using a semi-dry transfer unit (Amersham). The membranes were blocked with 5% non-fat milk in Tris-buffered saline containing 0.1% Tween 20 (TBS-T) for 1 hour at room temperature (RT), then incubated overnight at 4°C with the following primary antibodies in 5% milk-TBS: mouse monoclonal antibodies against phosphorylated (SMI31, Abcam, Cambridge, UK, 1:25,000), dephosphorylated (SMI32, Abcam, 1:3,000) and total (phosphorylated and unphosphorylated- N52, Sigma Aldrich, St. Louis, MO; 1:2,000) NF-heavy (NF-H), as well as against β-tubulin (E7; Developmental Studies Hybridoma Bank, DSHB, University of Iowa , Iowa City, IA, 1:3,000), tau (DSHB, 1:1,000), glyceraldehyde 3-phosphate dehydrogenase (GAPDH; Santa Cruz Biotechnology, Santa Cruz, CA, 1:3,000) or myelin basic protein (MBP) (Abcam, 1:5,000). After washing, immunoblots were incubated for 1 hour with appropriate HRP-conjugated secondary antisera (Jackson ImmunoResearch, West Grove, PA, diluted 1:5,000–1:10,000) in 5% milk-TBS-T. The bound antibody was visualized by enhanced chemiluminescence system (ECL Plus, Amersham). The intensity of the bands was measured with Tinascan version 2.07d and normalized for loading with GAPDH bands. Genotypes were compared with the paired *t*-test (95% confidence interval; 0.05 threshold).

Immunohistochemistry

Mice were anesthetized with Avertin according to institutionally approved protocols, then transcardially perfused with phosphate-buffered saline (PBS) followed by fresh 4% paraformaldehyde in 0.1 M PBS. Sciatic nerves were post-fixed for 30 minutes in the same fixative. Teased nerve fibers were prepared from both fixed and unfixed nerves, dried on SuperFrost Plus glass slides overnight at RT and stored at −20°C. Teased fibers were permeabilized in acetone (−20°C for 10 minutes) and incubated at RT with blocking solution of 5% bovine serumalbumin containing 0.5% Triton-X for 1 hour. The primary antibodies diluted in blocking solution were incubated overnight at 4°C with mouse monoclonal antibodies against contactin-associated protein (Caspr, 1:50; gift of Dr. Elior Peles, Weizmann Institute of Science, Israel), MBP (Abcam, 1:500), PanNav (Sigma, 1:50), Cx32 (1:50; Zymed-Invitrogen, Carlsbad, CA), SMI31 (Abcam; 1:5000), SMI32 (Abcam; 1:500), synaptotagmin (DSHB; 1:50), dynein (Santa Cruz, 1:100), kinesin- (KIF3a, BD Biosciences, San Jose, CA, 1:50) and tau (DSHB, 1:300), as well as rabbit antisera against MBP (1:100; Sigma), Nav1.6 (1:100; Alomone Labs, Jerusalem, Israel), Nav1.8 (Alomone; 1:100), Kv1.2 (1:200; Alomone), APP (Chemicon; Millipore, Temecula, CA, 1:300).

Quantitation of APP+ Teased Sciatic Nerve Fibers

Quantitation of APP+ teased sciatic nerve fibers was carried out after staining with a rabbit antiserum against APP, combined with monoclonal against Caspr or MBP. At least 75 randomly selected fibers per animal from at least 3 different animals were examined in each genotype and age group (2, 4, and 8 months). Fibers from both genotypes were teased and stained at the same time and scored for APP+ staining by 2 observers (N.V. and K.A.K.) who were blinded to the genotype. Fibers were considered to have positive staining for APP when there was strong and continuous APP immunoreactivity (IR) extending to more than 3 internodes. Counts were reproducible between observers and on repeated evaluation of the slides (performed twice). We compared the proportion of APP+ fibers in each genotype with the unpaired *t*-test.

Electron Microscopy

Deeply anesthetized 2-, 4- and 8-month-old mice were transcardially perfused with 0.9% saline followed by 2.5% glutaraldehyde in 0.1M PBS (pH 7.2). The femoral and sciatic nerves were dissected and further fixed overnight at 4°C and then osmicated, dehydrated, and embedded in Araldite resin. Transverse semi-thin sections (1 μm) were stained with alkaline toluidine blue. Ultrathin sections (80–100 nm) were counterstained with lead citrate and uranyl acetate, and examined in a JEOL JEM-1010 transmission electron microscope (JEOL Ltd, Tokyo, Japan).

Analysis of Myelination

Transverse semi-thin sections of the sciatic nerves were examined. All demyelinated, remyelinated and normally myelinated axons were counted using the following criteria: axons larger than 1 μm without a myelin sheath were considered demyelinated; axons with myelin sheaths that were <10% of the axonal diameter and/or axons that were surrounded by "onion bulbs" (circumferentially arranged Schwann cell processes and extracellular matrix) were considered remyelinated; the other myelinated axons were considered normally myelinated. All measurements were performed blindly with respect to the genotype. Proportions of abnormally myelinated fibers were compared with the Mann-Whitney *U* test (significance level: $p = 0.05$).

Analysis of Axon Profiles

Axon calibers were assessed in 2- and 4-month-old WT and *Gjb1*-null mice ($n = 3$ from each genotype) using the ImagePro Analyzer 6.3 (Media Cybernetics, MD). Digital images of femoral nerves were captured with the 20x objective. The total area of axons (sum of all axon transverse areas) within each nerve and the total number of axons were measured. Axons were further categorized and quantified according to their mean diameter into 8 classes (i.e. 1–2, 2–3, 3–4, 4–6, 6–8, 8–10, 10–12 and 12–14 μm). All results were compared with the *t*-test.

Ultrastructural Analysis

Ultrathin transverse and longitudinal sections of femoral motor nerves from at least 3 different WT and *Gjb1*-null mice at the age of 2 and 4 months were examined. Only normally myelinated large axons (6- to 8-μm-diameter) were analyzed. To count mitochondria, the entire axon cross section was photographed at x15,000 magnification. To measure the cytoskeleton elements, a series of x30,000 images were then obtained from at least 10 different axons in each nerve. NFs and microtubules were counted automatically from 3 to 5 different randomly selected 1 μm^2 areas in each axon using the ImagePro Plus analyzer. All measurements were performed blindly in regards to the genotype. The average numbers of NFs, microtubules and mitochondria per 1 μm^2 were obtained in each axon, mouse and genotype and their densities were compared between genotypes with the *t*-test.

Sciatic Nerve Ligations

Four month- old *Gjb1*-null mice and their WT littermates ($n = 4$ per genotype) were deeply anesthetized. The right sciatic nerve was exposed and 2 5/0 silk ligatures (SilkamR, Braun, Tuttlingen, Germany), approximately 5 mm apart, were placed immediately distal to the sciatic notch. The mice were killed 3 hours later and equal nerve segments (~1-cm-long) proximal and distal to the ligature were collected. The corresponding segments were also collected from the non-ligated contralateral sciatic along with samples of the lumbar spinal cord. Tissues were further processed for immunoblot analysis as above. The segments between the ligatures were collected separately, fixed for 30 minutes in 4%

paraformaldehyde and processed for immunohistochemistry for several proteins undergoing axonal transport as above.

Antibodies used for immunoblot analysis in nerve ligation experiments included mouse monoclonal against synaptic proteins SV2 (developed by Kathleen M. Buckley, DSHB; diluted: 1:500), synaptotagmin (mAb48; developed by Louis Reichardt, DSHB, diluted: 1:1,000) and synapsin (DSHB; 1:250, developed by Erich Buchner), and against Dynein intermediate chain (Santa-Cruz, 1:1,000), MBP (Abcam; 1:5,000), and GAPDH (Santa Cruz; 1: 3,000). Blots were incubated with appropriate secondary antibodies and developed as above. For quantification, the intensity of the bands was measured and synaptic vesicle protein bands were normalized for loading according to GAPDH bands. We then calculated the ratios of synaptic protein levels in proximal and distal segments from ligated compared to contralateral unligated nerves and analyzed the results from *Gjb1*-null and WT mice with paired *t*-tests.

RESULTS

Development of Demyelination in *Gjb1*-Null Nerves

The femoral nerves of *Gjb1*-null mice showed progressive, predominantly motor demyelinating neuropathy starting after 3 months of age (12,13), with ~7% abnormally myelinated fibers at 4 months (25). To assess the degree of demyelination in the sciatic nerve we analyzed epoxy sections at 2, 4 and 8 months of age. Compared to femoral motor nerves, sciatic nerves had fewer abnormally myelinated fibers: 0% at 2 months and 3% at 4 months (Fig. 1). To determine whether the molecular architecture of myelinated axons was affected, we immunostained teased fibers of 2- and 4-month old *Gjb1*-null sciatic nerves. All myelinated fibers had normal appearing, MBP+ myelin sheaths and all nodes of Ranvier were Nav1.6+ (Supplemental Fig. 2E, F). We did not detect nodal Nav1.8 staining (Supplemental Fig. 2G, H), which has been found in some abnormally myelinated fibers in Tr^J mice (31), whereas small-diameter dorsal root ganglion neurons were Nav1.8+ (data not shown). As previously reported (32), *Shaker*-type Kv1.1/1.2 potassium channels and Caspr2 were normally expressed at juxtaparanodes and Caspr was normally localized at paranodes (Supplemental Fig. 2A–D). Moreover, the internodal lengths were not significantly different between 4-month-old *Gjb1*-null mice and their WT littermates (Supplemental Fig. 3), further supporting the contention that demyelinated and remyelinated axons are scarce at this age.

Increased Packing Density and Progressive Dephosphorylation of NFs in *Gjb1*-Null Nerves

As a first step in determining whether axons were affected in *Gjb1*-null mice prior to the onset of demyelination, we performed a quantitative analysis of the axonal calibers in femoral motor nerves of 2- and 4-month-old littermates. Even at 2 months, the numbers of large (>8 μm diameter) axons were reduced in *Gjb1*-null nerves; this reduction was more prominent at 4 months (Fig. 2). In contrast, *Gjb1*-null nerves showed higher percentages of medium caliber fibers (4–8 μm diameter), suggesting a shift towards smaller axon diameter in the *Gjb1*-null mice without axonal loss. Consistent with this observation, total axonal area and total number of axons did not significantly change at these ages.

We next analyzed NF density by electron microscopy in large myelinated axons in femoral motor nerves (>6 μm), excluding axons sectioned near the nodal region as well as axons that were demyelinated or remyelinated. NF density at 2 months was significantly greater in the *Gjb1*-null (n = 4, 116.4 ± 6.1 NF/μm^2) vs. WT mice (n = 3, 92.9 ± 1.6 NF/μm^2) ($p = 0.0016$, 2-tailed *t*-test). NF density was further increased at 4 months (144 ± 6.3 NF/μm^2 in *Gjb1*-null (n = 5) vs. 89.9±5.6 NF/μm^2 in WT mice (n = 4) ($p < 0.001$). There were no significant differences in the density of microtubules or mitochondria (Fig. 3).

Because dephosphorylation is associated with tighter packing of NFs (33–35), we immunoblotted sciatic nerve lysates for dephosphorylated (SMI32) and phosphorylated (SMI31) NF-H. At least 3 *Gjb1*-null and 3 WT littermates were analyzed at 2 and 4 months of age. Nerve lysates from single animals were immunoblotted at least 3 times and the signal intensity relative to that of GAPDH was quantified. *Gjb1*-null nerves had significantly higher SMI32 signals vs. their WT littermates starting at 2 months (189.9 ± 47.5% of WT at 2 months, $p = 0.04$; and 150.2 ± 11.8% at 4 months, $p = 0.009$), demonstrating increased dephosphorylation of NF-H, with a simultaneous reduction of the SMI31 signals at 4 months (90.8 ± 23.9% of WT at 2 months, $p = 0.28$; 73.9 ± 7.9% at 4 months, $p = 0.014$) (Fig. 4A–D). *Gjb1*-null nerves also had reduced phosphorylation of NF-medium (NF-M) (Supplemental Fig. 4A). In line with these results, total NF levels did not significantly differ between genotypes (Supplemental Fig. 4B), but the proportion of phosphorylated NFs was significantly lower at both ages (at 2 months 72.1 ± 4.1% of total NF was phosphorylated in WT mice, and 55.3 ± 4.2% in *Gjb1*-null littermates, $p = 0.00033$. At 4 months, 75.6 ± 4.1% of total NF was phosphorylated in WT mice and 60.5 ± 3.7% in *Gjb1*-null littermates, $p = 0.015$). Dynein and kinesin levels were not significantly changed (data not shown), whereas tubulin levels were minimally reduced in *Gjb1*-null nerves at 4 months (94.2 ± 2.2% of WT; $p = 0.02$). MBP levels were similar between genotypes even at 4 months, in keeping with minimal demyelination at this age.

To corroborate these results we immunostained teased fibers from 2-, 4-, and 8-month-old *Gjb1*-null mice and their WT littermates for SMI32 and MBP. Compared to WT nerves, SMI32-IR was clearly increased in 2-month-old *Gjb1*-null nerves and appeared inhomogeneous and extended to several internodes of each axon. At 4 and 8 months of age, SMI32-IR was more intense, appearing to fill the entire internodes of many axons, especially the large ones, whereas thin axons showed lower SMI32-IR (Fig. 4E-H and data not shown). SMI32-IR fibers had normal-appearing MBP+ myelin sheaths at all ages, thereby demonstrating that these were not demyelinated.

Axonal Degeneration Occurs at Early Stages of Neuropathy in *Gjb1*-Null Mice

Because intra-axonal accumulation of APP is a marker of axonal degeneration (29), we next immunostained teased fibers from sciatic nerves of 2-, 4- and 8-month-old mice for APP. *Gjb1*-null mice had more APP+ axons than their WT littermates and the proportion of APP+ axons increased with age (Fig. 5). At 2 months,11.6 ± 5.2% in WT and 26.2 ± 2.0% of fibers in *Gjb1*-null were APP+ ($p = 0.027$, 2-tailed *t*-test for unpaired samples); at 4 months, 12.9 ± 6.9% in WT and 42.1 ± 11% in *Gjb1*-null were APP+ ($p = 0.022$); and at 8 months, 12.4 ± 5.5% in WT and 63.6 ± 8.0% in *Gjb1*-null were APP+ ($p = 0.014$). The pattern of MBP-IR surrounding the APP+ axons looked normal, indicating that myelination was normal. APP-IR was most pronounced in the paranodes and juxtaparanodes bordering the nodes of Ranvier, as shown by co-staining for the paranodal protein Caspr (Fig. 5 and data not shown).

Impairment of Axonal Transport in Gap Junction-Deficient Nerves

The accumulation of APP, which undergoes fast anterograde transport (36), suggested that axonal transport might be impaired in *Gjb1*-null nerves. To investigate this we ligated 1 sciatic nerve of 4-month-old *Gjb1*-null mice and their age-matched WT littermates; 2 ligatures were placed 5 mm apart and the mice were killed after 3 hours (Fig. 6A). We immunoblotted protein extracts of individual nerve segments immediately proximal and distal to the ligatures and the corresponding segments of the contralateral/unlesioned nerve for several proteins associated with synaptic vesicles that undergo both anterograde and retrograde transport (37–39). Therefore, they normally accumulate following nerve ligation, and this accumulation is diminished in nerves with impaired fast axonal transport (40,41).

The levels of synaptotagmin, SV2, and synapsin in the segment distal to the ligature were lower in *Gjb1*-null mice compared to their WT littermates, indicating that retrograde axonal transport was reduced (Fig. 6). We found similar results for nerves that had been ligated for 6 hours (not shown). In addition, the steady state levels of the same proteins (Fig. 6D), as well as of the microtubule associated protein tau (42) (Supplemental Fig. 6E), were higher in unlesioned nerves from *Gjb1*-null mice, consistent with slower axonal transport. Finally, the retrograde motor dynein accumulated in the segments distal to the ligation and was depleted from the segments proximal to the ligation in WT but not in the *Gjb1*-null nerves, further supporting the fact that axonal transport is impaired in mice deficient for Cx32 (Supplemental Fig. 5). Likewise, the anterograde motor kinesin (as well as tau) accumulated in segments proximal to the ligation in WT but much less in *Gjb1*-null nerves (Supplemental Fig. 6A–D). Taken together, these findings indicate that both anterograde and retrograde axonal transport is impaired in *Gjb1*-null nerves.

DISCUSSION

Here, we provide the first evidence of axonal pathology in early stages of neuropathy in *Gjb1*-null mice, a model of CMT1X. We find increased packing density and dephosphorylation of axonal NFs, accumulation of APP and synaptic vesicle-associated proteins, and diminished retrograde axonal transport before significant demyelination has occurred. These findings highlight novel aspects of CMT1X pathogenesis and emphasize the importance of Cx32 GJs in mediating Schwann cell-axonalinteractions.

Early Axonal Cytoskeleton Changes in *Gjb1*-Null Mice

NFs are the major cytoskeletal proteins in axons and are heteropolymers composed of 3 polypeptide subunits named according to their relative molecular weights, NF–H, NF–M and NF-light (NF-L) (43,44). In normal myelinated axons, the number of NFs correlates with the axonal size (45–47), and the lack of axonal NFs in quail, mice, or humans markedly reduces axonal calibers and conduction velocities (45–50). In addition to the number of NFs, the phosphorylation of the KSP (Lys-Ser-Pro) repeats in NF-H and NF-M increases their negative charge and thereby augments their lateral spacing and the formation of cross-bridges (34,35,51). In the PNS (52) and the CNS (51,53), increased spacing of NFs may contribute to the axonal diameter. However, eliminating phosphorylation of either NF-H (54,55) or NF-M KSP repeats (56) did not affect NF spacing and acquisition of normal axonal caliber, suggesting that NF-H and NF-M may have partially overlapping functions (57). Thus, it remains to be shown whether dephosphorylation of both NF-M and NF-H, as shown here in *Gjb1*-null mice, affects axon calibers.

How myelinating glia increase the number of axonal neurofilaments and their phosphorylation is not known. Both axonalkinases and phosphatases regulate NF-M and NF-H phosphorylation(58). Multiple signal transduction cascades (triggered by growth factors, Ca^{2+} influx, or integrins) and many different kinases (e.g. ERK1/2, Cdk5, p38 MAP kinase/SAPK) lead to phosphorylation (59–62). In the CNS, axonal ensheathment by oligodendrocytes appears to be sufficient to increase axonal diameter, but not to the same extent as myelination (63). In the PNS, myelin-associated glycoprotein (MAG) appears to play a crucial role. MAG is localized on the adaxonal membrane (and non-compact myelin) of myelinating Schwann cells (64) and interacts with lipids on apposing axonal membrane (65). PNS axons in *Mag*-null mice have relatively dephosphorylated and tightly packed axonal NF, which is associated with reduced axonal calibers (66). However, because it is normally localized in *Gjb1*-null mice (13), MAG is unlikely to mediate the effects of the loss of Cx32.

Altered Axonal Transport in *Gjb1*-Null Mice

Axonal transport is required for axonal growth, function and viability (67–69) and is accomplished by 2 sets of motor proteins: kinesins for anterograde transport and dynactin complex for retrograde transport. APP is axonally transported (70,71) and accumulates in a variety of demyelinating and neurodegenerative diseases in both rodents (72–75) and humans (76–78). Similarly, the microtubule associated tau undergoes slow axonal transport utilizing fast transport motors and is also known to accumulate in neurodegeneration (42). Thus, accumulation of APP, tau, and different synaptic vesicle-related proteins in unlesioned *Gjb1*-null nerves as shown here suggests impaired axonal transport before demyelination, which is further demonstrated by the results of nerve ligations.

It is possible that the perturbations of NFs we found diminish axonal transport. Mitochondria associate directly with NF sidearms and this interaction is mediated by NF phosphorylation as well as mitochondrial membrane potential (79,80). NF cross-bridging, which depends on phosphorylation (35), competes with kinesin-dependent association of NFs with microtubules (81). This may be a mechanism by which C-terminal NF phosphorylation contributes to slowing in axonal transport of NFs and axon stability since disruption of NF-H increases NF motility (82). Furthermore, cultured neurons from *Nefl*-null mice show abnormal mitochondrial distribution and motility, suggesting that the NF network regulates the trafficking of these organelles (83–84). Similarly, dephosphorylation of axonal NFs is associated with mitochondrial depletion in multiple sclerosis (78).

Axonal Pathology Occurs Independently of Demyelination

Closer spacing of NFs, less phosphorylation, and smaller axonal calibers are also seen in other demyelinating mutants (13,19,22,85–87). However, the cytoskeletal changes and defects in axonal transport in *Gjb1*-null mice occur in axons that appear to be normally myelinated, indicating dissociation of these axonal alterations from demyelination. This confirms and extends the list of axonal abnormalities that may occur independently of demyelination in other myelin mutants. For example, *Plp1*-null mice have impairment of fast axonal transport, despite being well myelinated (73). Degeneration of axons surrounded by normal appearing myelin sheaths has been found in *Plp1*-null (72) and *Cnp1*-null mice (88). In contrast, the CNS axons in *shiverer* mice, which are dysmyelinated due to lack of MBP, show no axonal pathology (89).

How the loss of GJs composed of Cx32 leads to axonal alterations remains unclear. Cx32 GJs provide a direct pathway of communication between the adaxonal and abaxonal Schwann cell cytoplasm (3). Perhaps the loss of a signal that depends on these GJs initiates the axonal alterations. The most well-developed possibilities are Ca^{2+} and IP3. The IP3-receptor-3 is also localized in the paranodal areas of Schwann cells (90). During neural activity, intracellular Ca^{2+} rises through the IP3 signalling cascade and undergoes ryanodin-dependent release from ER specifically at areas of non-compact myelin (91). In vitro studies showed that GJs allow the diffusion of Ca^{2+}-mobilizing second messengers across coupled cells (92) and intracellular calcium concentration regulates Cx32 hemichannel opening (93). It remains to be determined whether Cx32 GJs in non-compact myelin areas of myelinated fibers serve as conduits for the rapid radial spread of these Ca^{2+} and IP3 signals required for axonal integrity.

Supplementary Material

Refer to Web version on PubMed Central for supplementary material.

Acknowledgments

We thank Prof. Klaus Willecke for *Gjb1*-null mice and Prof. Elior Peles for the anti-Caspr antibody. The antibodies against SV2 (developed by Kathleen M. Buckley), synapsin (developed by Erich Buchner), synaptotagmin (developed by Louis Reichardt) and tau (developed by Gail V. W. Johnson) were obtained from the Developmental Studies Hybridoma Bank developed under the auspices of the NICHD and maintained by The University of Iowa, Department of Biology, Iowa City, Iowa. We also thank Sophia Aristodemou and Thalia Michael for technical assistance.

This work was supported by the Cyprus Telethon (Grant 2007-09 to KAK), the Cyprus Research Promotion Foundation (HEALTH/0506/04 to KAK), the National Multiple Sclerosis Society (USA) (Grant RG3457A2/1 to KAK), and the NIH (NS55284 and NS43174, to SSS).

References

1. Bergoffen J, Scherer SS, Wang S, et al. Connexin mutations in X-linked Charcot-Marie-Tooth disease. Science 1993;262:2039–42. [PubMed: 8266101]
2. Scherer SS, Deschênes SM, Xu Y-T, et al. Connexin32 is a myelin-related protein in the PNS and CNS. J Neurosci 1995;15:8281–94. [PubMed: 8613761]
3. Balice-Gordon RJ, Bone LJ, Scherer SS. Functional gap junctions in the Schwann cell myelin sheath. J Cell Biol 1998;142:1095–1104. [PubMed: 9722620]
4. Meier C, Dermietzel R, Davidson KG, et al. Connexin32-containing gap junctions in Schwann cells at the internodal zone of partial myelin compaction and in Schmidt-Lanterman incisures. J Neurosci 2004;24:3186–98. [PubMed: 15056698]
5. Kleopa KA, Scherer SS. Molecular genetics of X-linked Charcot-Marie-Tooth disease. Neuromolecular Med 2006;8:107–122. [PubMed: 16775370]
6. Hahn AF, Ainsworth PJ, Bolton CF, et al. Pathological findings in the X-linked form of Charcot-Marie-Tooth disease: A morphometric and ultrastructural analysis. Acta Neuropathol 2001;101:129–39. [PubMed: 11271367]
7. Hahn AF, Brown WF, Koopman WJ, et al. X-linked dominant hereditary motor and sensory neuropathy. Brain 1990;113:1511–25. [PubMed: 2245309]
8. Nicholson G, Nash J. Intermediate nerve conduction velocities define X-linked Charcot-Marie-Tooth neuropathy families. Neurology 1993;43:2558–64. [PubMed: 8255457]
9. Hattori N, Yamamoto M, Yoshihara T, et al. Demyelinating and axonal features of Charcot-Marie-Tooth disease with mutations of myelin-related proteins (PMP22, MPZ and Cx32): A clinicopathological study of 205 Japanese patients. Brain 2003;126:134–51. [PubMed: 12477701]
10. Kleopa KA, Zamba-Papanicolaou E, Alevra X, et al. Phenotypic and cellular expression of two novel connexin32 mutations causing CMT1X. Neurology 2006;66:396–402. [PubMed: 16476939]
11. Krajewski KM, Lewis RA, Fuerst DR, et al. Neurological dysfunction and axonal degeneration in Charcot-Marie–Tooth disease. Brain 2000;123:1516–27. [PubMed: 10869062]
12. Anzini P, Neuberg DH-H, Schachner M, et al. Structural abnormalities and deficient maintenance of peripheral nerve myelin in mice lacking the gap junction protein connexin32. J Neurosci 1997;17:4545–61. [PubMed: 9169515]
13. Scherer SS, Xu Y-T, Nelles E, et al. Connexin32-null mice develop a demyelinating peripheral neuropathy. Glia 1998;24:8–20. [PubMed: 9700485]
14. Sancho S, Magyar JP, Aguzzi A, et al. Distal axonopathy in peripheral nerves of PMP22 mutant mice. Brain 1999;122:1563–77. [PubMed: 10430839]
15. Suter U, Welcher AA, Ozcelik T, et al. Trembler mouse carries a point mutation in a myelin gene. Nature 1992;356:241–44. [PubMed: 1552943]
16. Henry EW, Cowen JS, Sidman RL. Comparison of Trembler and Trembler-J phenotypes: Varying severity of peripheral hypomyelination. J Neuropathol Exp Neurol 1983;42:688–706. [PubMed: 6313869]
17. Martini R, Zielasek J, Toyka KV, et al. Protein zero (P0)-deficient mice show myelin degeneration in peripheral nerves characteristic of inherited human neuropathies. Nature Genet 1995;11:281–5. [PubMed: 7581451]

18. Giese KP, Martini R, Lemke G, et al. Mouse P_0 gene disruption leads to hypomyelination, abnormal expression of recognition molecules, and degeneration of myelin and axons. Cell 1992;71:565–76. [PubMed: 1384988]
19. de Waegh S, Brady SB. Altered slow axonal transport and regeneration in a myelin-deficient mutant mouse: The Trembler as an in vivo model for Schwann cell-axon interactions. J Neurosci 1990;10:1855–65. [PubMed: 2355253]
20. Watson DF, Nachtman FN, Kuncl RW, et al. Altered neurofilament phosphorylation and beta tubulin isotypes in Charcot-Marie-Tooth disease type 1. Neurology 1994;44:2383–7. [PubMed: 7991130]
21. Aguayo AJ, Attiwell M, Trecarten J, et al. Abnormal myelination in transplanted Trembler mouse Schwann cells. Nature 1977;265:73–5. [PubMed: 189201]
22. de Waegh SM, Lee VM-Y, Brady ST. Local modulation of neurofilament phosphorylation, axonal caliber, and slow axonal transport by myelinating Schwann cells. Cell 1992;68:451–63. [PubMed: 1371237]
23. Sahenk Z, Chen L, Mendell JR. Effects of PMP22 duplication and deletions on the axonal cytoskeleton. Ann Neurol 1999;45:16–24. [PubMed: 9894872]
24. Sahenk Z, Chen L. Abnormalities in the axonal cytoskeleton induced by a connexin32 mutation in nerve xenografts. J Neurosci Res 1998;51:174–84. [PubMed: 9469571]
25. Sargiannidou I, Vavlitou N, Aristodemou S, et al. Connexin32 mutations cause loss of function in Schwann cells and oligodendrocytes leading to PNS and CNS myelination defects. J Neurosci 2009;29:4748–61.
26. Ainsworth PJ, Bolton CF, Murphy BC, et al. Genotype/phenotype correlation in affected individuals of a family with a deletion of the entire coding sequence of the connexin 32 gene. Hum Genet 1998;103:242–4. [PubMed: 9760211]
27. Nakagawa M, Takashima H, Umehara F, et al. Clinical phenotype in X-linked Charcot-Marie-Tooth disease with an entire deletion of the connexin 32 coding sequence. J Neurol Sci 2001;185:31–6. [PubMed: 11266688]
28. Shy ME, Siskind C, Swan ER, et al. CMT1X phenotypes represent loss of GJB1 gene function. Neurology 2007;68:849–55. [PubMed: 17353473]
29. Kuhlmann T, Lingfeld G, Bitsch A, et al. Acute axonal damage in multiple sclerosis is most extensive in early disease stages and decreases over time. Brain 2002;125:2202–12. [PubMed: 12244078]
30. Nelles E, Butzler C, Jung D, et al. Defective propagation of signals generated by sympathetic nerve stimulation in the liver of connexin32-deficient mice. Proc Natl Acad Sci USA 1996;93:9565–70. [PubMed: 8790370]
31. Devaux JJ, Scherer SS. Altered ion channels in an animal model of Charcot-Marie-Tooth disease type IA. J Neurosci 2005;25:1470–80. [PubMed: 15703401]
32. Arroyo EJ, Xu Y-T, Zhou L, et al. Myelinating Schwann cells determine the internodal localization of Kv1.1, Kv1.2, Kvβ2, and Caspr. J Neurocytol 1999;28:333–47. [PubMed: 10739575]
33. Mata M, Kupina N, Fink DJ. Phosphorylation-dependent neurofilament epitopes are reduced at the node of Ranvier. J Neurocytol 1992;21:199–210. [PubMed: 1373184]
34. Gotow T, Tanaka T, Nakamura Y, et al. Dephosphorylation of the largest neurofilament subunit protein influences the structure of crossbridges in reassembled neurofilaments. J Cell Sci 1994;107:1949–57. [PubMed: 7983161]
35. Julien J-P. Neurofilament functions in health and disease. Curr Opin Neurobiol 1999;9:554–60. [PubMed: 10508735]
36. Lazarov O, Morfini GA, Pigino G, et al. Impairments in fast axonal transport and motor neuron deficits in transgenic mice expressing familial Alzheimer's disease-linked mutant presenilin 1. J Neurosci 2007;27:7011–20. [PubMed: 17596450]
37. Dahlström AB, Czernik AJ, Li JY. Organelles in fast axonal transport. What molecules do they carry in anterograde vs retrograde directions, as observed in mammalian systems? Mol Neurobiol 1992;6:157–77. [PubMed: 1282329]

38. Okada Y, Yamazaki H, Sekine-Aizawa Y, et al. The neuron-specific kinesin superfamily protein KIF1A is a unique monomeric motor for anterograde axonal transport of synaptic vescle precursors. Cell 1995;81:769–80. [PubMed: 7539720]
39. Goldstein LS, Yang Z. Microtubule-based transport systems in neurons: the roles of kinesins and dyneins. Annu Rev Neurosci 2000;23:39–71. [PubMed: 10845058]
40. Kamal A, Stokin GB, Yang Z, et al. Axonal transport of amyloid precursor protein is mediated by direct binding to the kinesin light chain subunit of kinesin-I. Neuron 2000;28:449–59. [PubMed: 11144355]
41. Zhao C, Takita J, Tanaka Y, et al. Charcot-Marie-Tooth disease type 2A caused by mutation in a microtubule motor KIF1Bb. Cell 2001;105:587–97. [PubMed: 11389829]
42. Utton MA, Noble WJ, Hill JE, et al. Molecular motors implicated in the axonal transport of tau and alpha-synuclein. J Cell Sci 2005;118:4645–54. [PubMed: 16176937]
43. Hoffman PN, Lasek RJ. The slow component of axonal transport. Identification of major structural polypeptides of the axon and their generality among mammalian neurons. J Cell Biol 1975;66:351–66. [PubMed: 49355]
44. Julien J-P, Meyer D, Flavell D, et al. Cloning and developmental expression of the murine neurofilament gene family. Mol Brain Res 1986;1:243–50.
45. Friede RL, Samorajski T. Axon caliber related to neurofilaments and microtubules in sciatic nerve fibers of rats and mice. Anat Rec 1970;167:379–88. [PubMed: 5454590]
46. Muma NA, Hoffman PN. Neurofilaments are intrinsic determinants of axonal caliber. Micron 1993;24:677–83.
47. Ohara O, Gahara Y, Miyake T, et al. Neurofilament deficiency in quail caused by nonsense mutation in neurofilament-L gene. J Cell Biol 1993;121:387–95. [PubMed: 8468353]
48. Eyer J, Peterson A. Neurofilament-deficient axons and perikaryal aggregates in viable transgenic mice expressing a neurofilament--galactosidase fusion protein. Neuron 1994;12:389–405. [PubMed: 8110465]
49. Zhu Q, Couillard-Despres S, Julien JP. Delayed maturation of regenerating myelinated axons in mice lacking neurofilaments. Exp Neurol 1997;148:299–316. [PubMed: 9398473]
50. Yum SW, Zhang J, Mo K, et al. A novel recessive NEFL mutation causes a severe, early-onset axonal neuropathy. Ann Neurol 2009;66:759–70. [PubMed: 20039262]
51. Nixon RA, Paskevich PA, Sihag RK, et al. Phosphorylation on carboxyl terminus domains of neurofilament proteins in retinal ganglion cell neurons in vivo: Influences on regional neurofilament accumulation, interneurofilament spacing, and axon caliber. J Cell Biol 1994;126:1031–46. [PubMed: 7519617]
52. Hsieh S-T, Kidd GJ, Crawford TO, et al. Regional modulation of neurofilament organization by myelination in normal axons. J Neurosci 1994;14:6392–6401. [PubMed: 7965044]
53. Sanchez I, Hassinger L, Sihag RK, et al. Local control of neurofilament accumulation during radial growth of myelinating axons in vivo: Selective role of site-specific phosphorylation. J Cell Biol 2000;151:1013–24. [PubMed: 11086003]
54. Rao MV, Houseweart MK, Williamson TL, et al. Neurofilament-dependent radial growth of motor axons and axonal organization of neurofilaments does not require the neurofilament heavy subunit (NF-H) or its phosphorylation. J Cell Biol 1998;143:171–81. [PubMed: 9763429]
55. Rao MV, Garcia ML, Miyazaki Y, et al. Gene replacement in mice reveals that the heavily phosphorylated tail of neurofilament heavy subunit does not affect axonal caliber or the transit of cargoes in slow axonal transport. J Cell Biol 2002;158:681–93. [PubMed: 12186852]
56. Garcia ML, Rao MV, Fujimoto J, et al. Phosphorylation of highly conserved neurofilament medium KSP repeats is not required for myelin-dependent radial axonal growth. J Neurosci 2009;29:1277–84. [PubMed: 19193875]
57. Garcia ML, Lobsiger CS, Shah SB, et al. NF-M is an essential target for the myelin-directed “outside-in” signaling cascade that mediates radial axonal growth. J Cell Biol 2003;163:1011–20. [PubMed: 14662745]
58. Pant HC, Veeranna. Neurofilament phosphorylation. Biochem Cell Biol 1995;73:575–92. [PubMed: 8714676]

59. Li B, Veeranna, Grant P, et al. Calcium influx and membrane depolarization induce phosphorylation of neurofilament (NF-M) KSP repeats in PC12 cells. Brain Res Mol Brain Res 1999;70:84–91. [PubMed: 10381546]
60. Sun D, Leung CL, Liem RKH. Phosphorylation of the high molecular weight neurofilament protein (NF-H) by Cdk5 and p35. J Biol Chem 1996;271:14245–51. [PubMed: 8662984]
61. Veeranna V, Amin ND, Ahn NG, et al. Mitogen-activated protein kinases (Erk1, 2) phosphorylate Lys-Ser-Pro (KSP) repeats in neurofilament proteins NF-H and NFM. J Neurosci 1998;18:4008–21. [PubMed: 9592082]
62. Sihag PK, Inagaki M, Yamaguchi T, et al. Role of Phosphorylation on the structural dynamics and function of types iii and iv intermediate filaments. Exp Cell Res 2007;313:2098–2109. [PubMed: 17498690]
63. Sanchez I, Hassinger L, Paskevich PA, et al. Oligodendroglia regulate the regional expansion of axon caliber and local accumulation of neurofilaments during development independently of myelin formation. J Neurosci 1996;16:5095–5105. [PubMed: 8756439]
64. Trapp BD, Quarles RH. Presence of the myelin-associated glycoprotein correlates with alterations in the periodicity of peripheral myelin. J Cell Biol 1982;92:877–82. [PubMed: 6177705]
65. Schnaar RL, Lopez PH. Myelin-associated glycoprotein and its axonal receptors. J Neurosci Res 2009;87:3267–76. [PubMed: 19156870]
66. Yin XH, Crawford TO, Griffin JW, et al. Myelin-associated glycoprotein is a myelin signal that modulates the caliber of myelinated axons. J Neurosci 1998;18:1953–62. [PubMed: 9482781]
67. Chevalier-Larsen E, Holzbaur EL. Axonal transport and neurodegenerative disease. Biochim Biophys Acta 2006;1762:1094–1108. [PubMed: 16730956]
68. Duncan JE, Goldstein LS. The genetics of axonal transport and axonal transport disorders. PLoS Genet 2006;2:1275–84.
69. Hirokawa N, Noda Y. Intracellular transport and kinesin superfamily proteins, KIFs: structure, function, and dynamics. Physiol Rev 2008;88:1089–1118. [PubMed: 18626067]
70. Koo EH, Sisodia SS, Archer DR, et al. Precursor of amyloid protein in Alzheimer disease undergoes fast anterograde axonal transport. Proc Natl Acad Sci USA 1990;87:1561–5. [PubMed: 1689489]
71. Sisodia SS, Koo EH, Hoffman PN, et al. Identification and transport of full-length amyloid precursor proteins in rat peripheral nervous system. J Neurosci 1993;13:3136–42. [PubMed: 8331390]
72. Griffiths I, Klugmann M, Anderson T, et al. Axonal swellings and degeneration in mice lacking the major proteolipid of myelin. Science 1998;280:1610–13. [PubMed: 9616125]
73. Edgar JM, McLaughlin M, Yool D, et al. Oligodendroglial modulation of fast axonal transport in a mouse model of hereditary spastic paraplegia. J Cell Biol 2004;166:121–31. [PubMed: 15226307]
74. Seehusen F, Baumgärtner W. Axonal pathology and loss precede demyelination and accompany chronic lesions in a spontaneously occurring animal model of multiple sclerosis. Brain Pathol 2010;20:551–9. [PubMed: 19775292]
75. Her LS, Goldstein LS. Enhanced sensitivity of striatal neurons to axonal transport defects induced by mutant huntingtin. J Neurosci 2008;28:13662–72. [PubMed: 19074039]
76. Ferguson B, Matyszak MK, Esiri MM, et al. Axonal damage in acute multiple sclerosis lesions. Brain 1997;120:393–9. [PubMed: 9126051]
77. Bitsch A, Schuchardt J, Bunkowski S, et al. Acute axonal injury in multiple sclerosis -Correlation with demyelination and inflammation. Brain 2000;123:1174–83. [PubMed: 10825356]
78. Mahad DJ, Ziabreva I, Campbell G, et al. Mitochondrial changes within axons in multiple sclerosis. Brain 2009;132:1161–74. [PubMed: 19293237]
79. Ackerley S, Thornhill P, Grierson AJ, et al. Neurofilament heavy chain side arm phosphorylation regulates axonal transport of neurofilaments. J Cell Biol 2003;161:489–95. [PubMed: 12743103]
80. Wagner OI, Lifshitz J, Janmey PA, et al. Mechanisms of mitochondria-neurofilament interactions. J Neurosci 2003;23:9046–58. [PubMed: 14534238]

81. Kushkuley J, Chan WK, Lee S, et al. Neurofilament cross-bridging competes with kinesin-dependent association of neurofilaments with microtubules. J Cell Sci 2009;122:3579–86. [PubMed: 19737816]
82. Zhu QZ, Lindenbaum M, Levavasseur F, et al. Disruption of the NF-H gene increases axonal microtubule content and velocity of neurofilament transport: Relief of axonopathy resulting from the toxin beta,beta'-iminodipropionitrile. J Cell Biol 1998;143:183–93. [PubMed: 9763430]
83. Pérez-Ollé R, López-Toledano M, Goryunov D, et al. Mutations in the neurofilament light gene linked to Charcot-Marie-Tooth disease cause defects in transport. J Neurochem 2005;93:861–74. [PubMed: 15857389]
84. Perrot R, Julien JP. Real-time imaging reveals defects of fast axonal transport induced by disorganization of intermediate filaments. FASEB J 2009;23:3213–25. [PubMed: 19451279]
85. Cole JS, Messing A, Trojanowski JQ, et al. Modulation of axon diameter and neurofilaments by hypomyelination Schwann cells in transgenic mice. J Neurosci 1994;14:6956–66. [PubMed: 7965091]
86. de Waegh S, Brady SB. Local control of axonal properties by Schwann cells: Neurofilaments and axonal tranport in homologous and heterologous nerve grafts. J Neurosci Res 1991;30:201–12. [PubMed: 1795404]
87. Kirkpatrick L, Brady ST. Modulation of the axonal microtubule cytoskeleton by myelinating Schwann cells. J Neurosci 1994;14:7440–50. [PubMed: 7996186]
88. Lappe-Siefke C, Goebbels S, Gravel M, et al. Disruption of Cnp1 uncouples oligodendroglial functions in axonal support and myelination. Nat Genet 2003;33:366–74. [PubMed: 12590258]
89. Edgar JM, McLaughlin M, Werner HB, et al. Early ultrastructural defects of axons and axon-glia junctions in mice lacking expression of Cnp1. Glia 2009;57:1815–24. [PubMed: 19459211]
90. Toews JC, Schram V, Weerth SH, et al. Signaling proteins in the axoglial apparatus of sciatic nerve nodes of Ranvier. Glia 2007;55:202–13. [PubMed: 17091480]
91. Lev-Ram V, Ellisman MH. Axonal activation-induced calcium transients in myelinating Schwann cells, sources, and mechanisms. J Neurosci 1995;15:2628–37. [PubMed: 7722618]
92. Anselmi F, Hernandez VH, Crispino G, et al. ATP release through connexin hemichannels and gap junction transfer of second messengers propagate Ca2+ signals across the inner ear. Proc Natl Acad Sci U S A 2008;105:18770–5. [PubMed: 19047635]
93. De Vuyst E, Decrock E, Cabooter L, et al. Intracellular calcium changes trigger connexin 32 hemichannel opening. EMBO J 2006;25:34–44. [PubMed: 16341088]

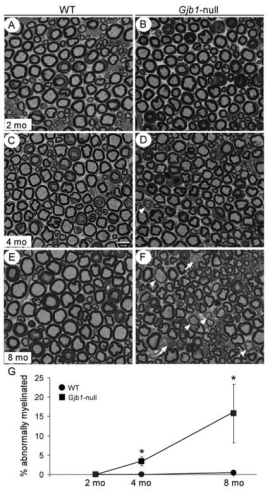

Figure 1.

Sciatic nerve demyelination in *Gjb1*-null mice is minimal up to 4 months of age. (**A–F**) Semithin sections from 2- (**A, B**), 4- (**C, D**) and 8-month-old (**E, F**) wild type (WT) (**A, C, E**) and *Gjb1*-null (B, D, F) mice. In *Gjb1*-null sciatic nerves there are no demyelinated or remyelinated axons at 2 months of age. Abnormally myelinated axons are rare at 4 months (**D**), and become more numerous at 8 months (**F**), including demyelinated (arrows) and remyelinated (arrowheads). Bar = 10 μm. (**G**) Quantitative analysis of sciatic nerve myelination in WT and *Gjb1*-null mice at 2, 4, and 8 months of age (n = 4 per genotype and age group) shows very mild demyelination in *Gjb1*-null mice at 4 months with 3.4 ± 1.2% (average ± SD) of fibers being abnormally myelinated vs. none in WT, ($p = 0.01$, Mann-Whitney U test); by 8 months there is progression (15.7 ± 7.6% of fibers abnormally myelinated vs. 0.4 ± 0.5% in WT; $p = 0.03$).

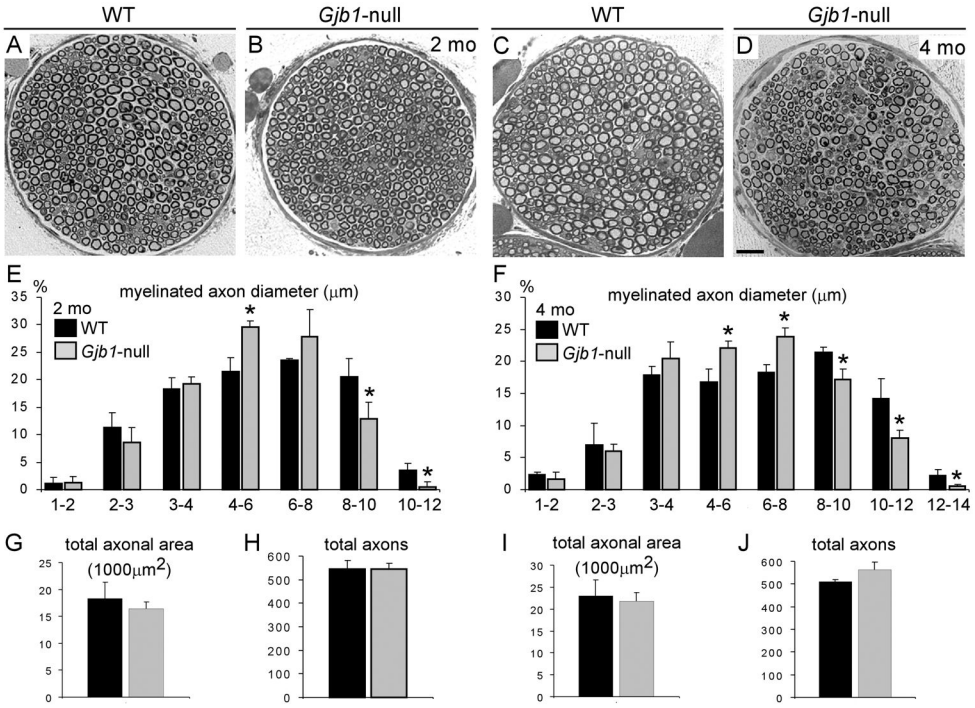

Figure 2.

Reduced axonal diameters in *Gjb1*-null mice. (**A–D**) Representative semithin sections of femoral motor nerves from 2- (**A, B**) and 4-month-old (**C, D**) wild type (WT) (**A, C**) and *Gjb1*-null (**B, D**) mice. A few axons are demyelinated or remyelinated at 4 months of age in *Gjb1*-null nerves. Scale bar = 20 μm. (**E–J**) Quantitative analysis of axon diameters (**E, F**), total axonal area (**G, I**), and total numbers of axons (**H, J**) in WT and *Gjb1*-null mice (n = 3 per age group and genotype) at 2 months (**E, G, H**) and 4 months (**F, I, J**). At both ages the percentages of large myelinated fibers (>8μm) is reduced in *Gjb1*-null vs. WT nerves. In contrast, *Gjb1*-null nerves show higher percentages of medium sized fibers (4 to 6 μm at 2 months; 4 to 8 μm at 4 months). The total axonal area and the total number of axons are not significantly changed in *Gjb1*-null nerves, suggesting a shift to smaller diameters without axonal loss. *Indicates significant differences (2-tailed t-test).

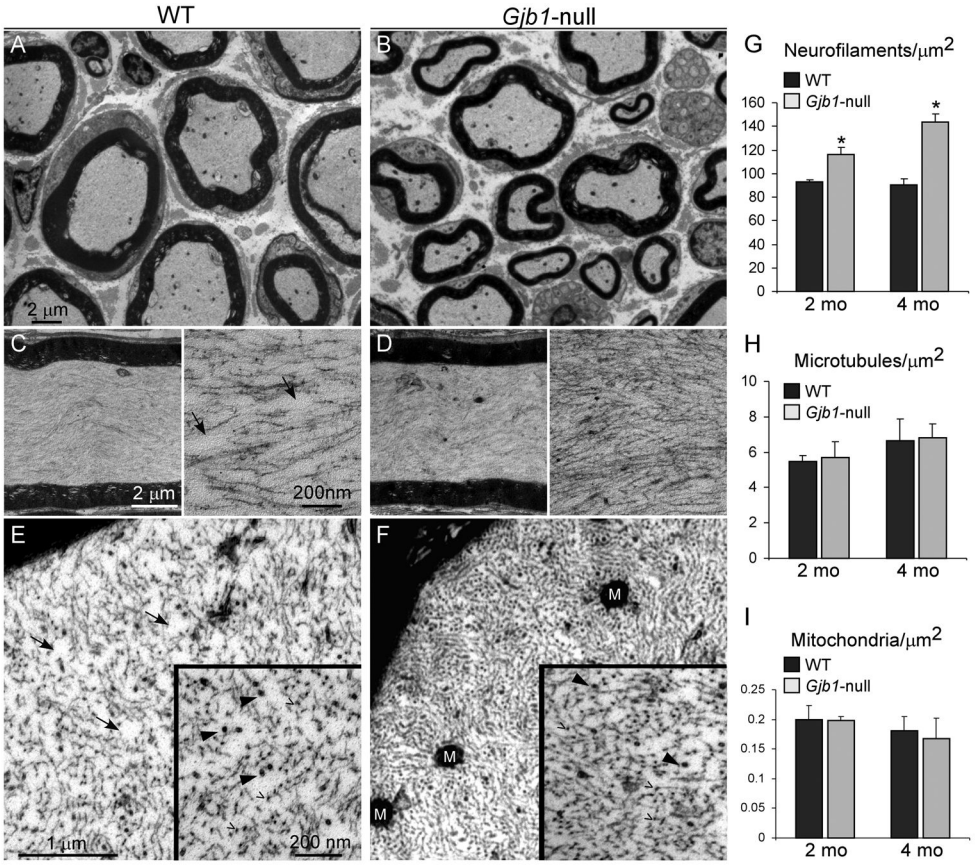

Figure 3.

Increased density of axonal neurofilaments in *Gjb1*-null femoral nerves. (**A–F**) Electron micrographs from femoral motor nerves of 4-month-old wild type (WT) (**A, C, E**) and *Gjb1*-null (**B, D, F**) mice. Low-magnification images (**A, B**) show that axons are normally myelinated in *Gjb1*-null nerve. Higher magnification images of longitudinal (**C, D**) and transverse (**E, F**) sections of normally myelinated axons illustrate the higher density of neurofilaments (NFs) in the *Gjb1*-null vs. the WT axons. At higher magnification of longitudinal (insets, **C, D**) and transverse sections (insets, **E, F**), NFs (open arrowheads) appear more tightly packed in *Gjb1*-null axons; microtubules (arrowheads) do not show clear differences in density. Areas devoid of NFs seen in the WT (arrows in **C** and **E**) are absent in the *Gjb1*-null (**D, F**). M = mitochondria. (**G–I**) Average density per μm^2 of NFs (**G**), microtubules (**H**) and mitochondria (**I**) obtained in at least 10 normally myelinated axons (6-to 8-μm diameter) from 2- and 4-month-old mice in each genotype (n = 3–5 mice per genotype and age group). The density of NFs is higher in *Gjb1*-null mice vs. WT starting at 2 months and is further increased at 4 months. The densities of microtubules and mitochondria are not significantly different at any age (*Indicates significant results).

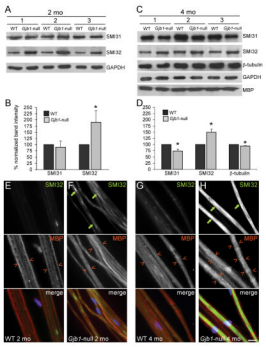

Figure 4.

Early dephosphorylation of axonal neurofilaments in *Gjb1*-null nerves without demyelination. (**A–D**) Immunoblot analysis of cytoskeletal components in sciatic nerves from 3 pairs of 2-month-old (**A, B**) and 4 month-old (**C, D**) wild (WT) and *Gjb1*-null littermates. (**A, C**) Representative blots are shown for antibodies to phosphorylated (SMI31) and non-phosphorylated (SMI32) NF-heavy (NF-H; 200 kDa) and β-tubulin (55 kDa) and glyceraldehyde 3-phosphate dehydrogenase (GAPDH) (37 kDa, loading control) and myelin basic protein (MBP, 20 kDa). In all pairs, SMI32 levels are greater in *Gjb1*-null vs. WT littermates. At 2 months SMI31 levels are not different, but at 4 months, SMI31 levels appear reduced, along with minimal reduction of β-tubulin; MBP levels are unchanged. (**B, D**) Results of quantitative analysis (average band intensity values for cytoskeletal proteins from at least 3 pairs of WT and *Gjb1*-null mice each run at least 3 times in SDS-PAGE and electrotransferred onto nitrocellulose for immunolabeling, normalized for loading to GAPDH). Non-phosphorylated NF-H levels are significantly greater in *Gjb1*-null nerves while phosphorylated NF-H levels are decreased at 4 months. β-tubulin levels are mildly reduced in *Gjb1*-null nerves at 4 months. *Indicates significant results ($p < 0.05$, paired t-test). (**E–H**) Immunostaining of sciatic nerve teased fibers for SMI32 (green) and MBP (red); cell nuclei are stained with DAPI (blue). Axons from 2-month-old *Gjb1*-null mice (**F**) have more SMI32-immunoreactivity (IR) (green arrows) than those from WT littermates (**E**), with inhomogeneous pattern along the entire axons. At 4 months, SMI32-IR completely fills some axons (**H**) of *Gjb1*-null mice. The SMI32+ axons have normal-appearing, MBP+ myelin sheaths (red open arrowheads). Scale bar in **H**: 10 μm.

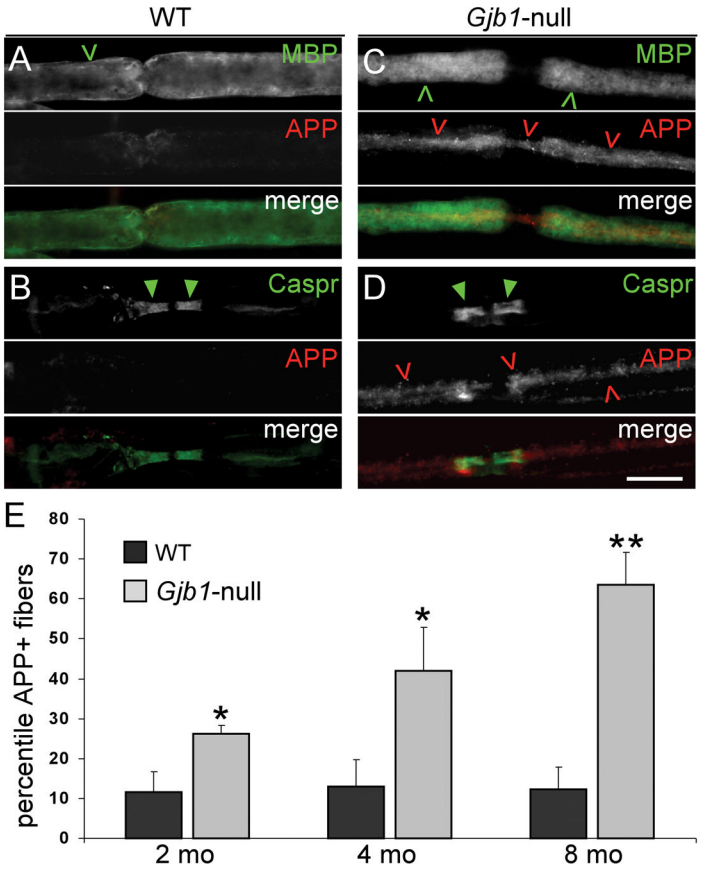

Figure 5.

Amyloid precursor protein (APP)+ axons in *Gjb1*-null sciatic nerves. (**A**–**D**) Representative images of teased fibers from 4-month-old wild type (WT) (**A, B**) and *Gjb1*-null (**C, D**) mice, double labeled with antibodies to APP (red) and either myelin basic protein (MBP, green, **A, C**) or contactin-associated protein (Caspr, green, **B, D**). Many *Gjb1*-null axons (red open arrowheads), but not WT axons, are APP+; these are surrounded by normal-appearing MBP + myelin sheaths (green open arrowheads) and have normal-appearing Caspr+ paranodes (green arrowheads). Scale bar: 10 μm. (**E**) Quantitative analysis of APP+ axons in 2-, 4-, and 8-month old mice (n = 3 or 4 in each genotype and age group). The percentile of APP+ axons increases with age and, at every age, is significantly higher in *Gjb1*-null vs. WT mice.

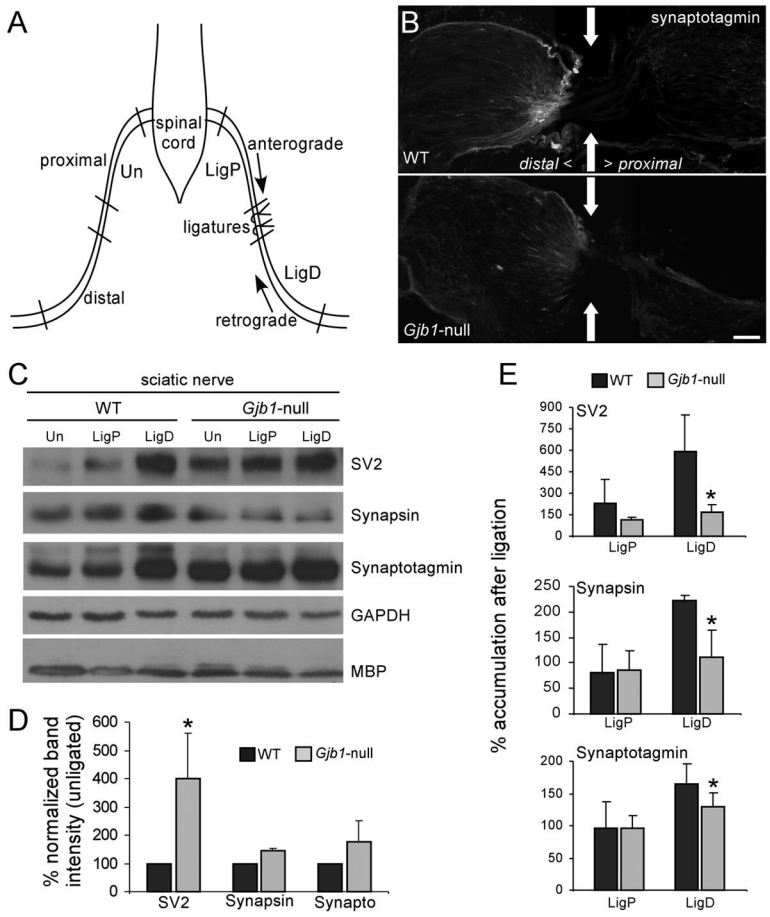

Figure 6.

Early impairment of axonal transport in *Gjb1*-null mice. (**A**) Schematic of the sciatic nerve ligation experiment. One sciatic nerve was doubly ligated; 3 hours later, segments proximal (LigP) and distal (LigD) to the ligation and the corresponding segments of the contralateral/unligated nerve (Un) were collected. (**B**) Immunostaining at the distal ligation site (arrows) shows more synaptotagmin accumulation in the wild type (WT) than in the *Gjb1*-null nerve. Bar = 40 μm. (**C**) Representative immunoblots of lysates from ligated (LigP and LigD) and unligated nerves, from WT and *Gjb1*-null mice. Membranes were blotted with monoclonal antibodies to SV2 (95 kDa), synapsin (70 kDa) and synaptotagmin (65 kDa), glyceraldehyde 3-phosphate dehydrogenase (GAPDH, loading control) and myelin basic protein (MBP) (20 kDa). The levels of SV2, synapsin and synaptotagmin in LigD (vs. same region of unligated nerves) are higher in WT than in *Gjb1*-null nerves; their steady state levels in unligated nerves are higher in the *Gjb1*-null. GADPH and MBP levels are similar in WT and *Gjb1*-null mice. (**D, E**) Quantitative results from 3 independent experiments. (**D**) Bars represent average percentage increase in synaptic protein levels (normalized for GAPDH signals) in unligated nerves from *Gjb1*-null vs. WT mice. (**E**) Bars represent average percentage increase in the synaptic protein levels in LigD and LigP vs. the contralateral unligated nerves, after normalization for GAPDH signals. SV2, synapsin, and synaptotagmin levels are significantly higher in WT vs. the *Gjb1*-null LigD segments (1-tailed paired t-test).